Title	Nanofibrous collagen nerve conduits for spinal cord repair.
Author(s)	Liu, T; Houle, JD; Xu, J; Chan, BP; Chew, SY
Citation	Tissue Engineering. Part A, 2012, v. 18 n. 9-10, p. 1057-1066
Issued Date	2012
URL	http://hdl.handle.net/10722/164262
Rights	This is a copy of an article published in the Tissue Engineering. Part A © 2012 copyright Mary Ann Liebert, Inc.; Tissue Engineering. Part A is available online at: http://www.liebertonline.com.

TISSUE ENGINEERING: Part A
Volume 18, Numbers 9 and 10, 2012

DOI: 10.1089/ten.tea.2011.0430

Nanofibrous Collagen Nerve Conduits for Spinal Cord Repair

Ting Liu, M.D.,[1] John D. Houle, Ph.D.,[2] Jinye Xu, M.Eng.,[3] Barbara P. Chan, Ph.D.,[3] and Sing Yian Chew, Ph.D.[1]

Nerve regeneration in an injured spinal cord is often restricted, contributing to the devastating outcome of neurologic impairment below the site of injury. Although implantation of tissue-engineered scaffolds has evolved as a potential treatment method, the outcomes remain sub-optimal. One possible reason may be the lack of topographical signals from these constructs to provide contact guidance to invading cells or regrowing axons. Nanofibers mimic the natural extracellular matrix architecturally and may therefore promote physiologically relevant cellular phenotypes. In this study, the potential application of electrospun collagen nanofibers (diameter = 208.2 ± 90.4 nm) for spinal cord injury (SCI) treatment was evaluated *in vitro* and *in vivo*. Primary rat astrocytes and dorsal root ganglias (DRGs) were seeded on collagen-coated glass cover slips (two-dimensional [2D] substrate controls), and randomly oriented or aligned collagen fibers to evaluate scaffold topographical effects on astrocyte behavior and neurite outgrowth, respectively. When cultured on collagen nanofibers, astrocyte proliferation and expression of glial fibrillary acidic protein (*GFAP*) were suppressed as compared to cells on 2D controls at days 3 ($p < 0.05$) and 7 ($p < 0.01$). Aligned fibers resulted in elongated astrocytes (elongation factor > 4, $p < 0.01$) and directed the orientation of neurite outgrowth from DRGs along fiber axes. In the contrast, neurites emanated radially on randomly oriented collagen fibers. By forming collagen scaffolds into spiral tubular structures, we demonstrated the feasibility of using electrospun nanofibers for the treatment of acute SCI using a rat hemi-section model. At days 10 and 30 postimplantation, extensive cellular penetration into the constructs was observed regardless of fiber orientation. However, scaffolds with aligned fibers appeared more structurally intact at day 30. *ED1* immunofluorescent staining revealed macrophage invasion by day 10, which decreased significantly by day 30. Neural fiber sprouting as evaluated by neurofilament staining was observed as early as day 10. In addition, *GFAP* immunostained astrocytes were found only at the boundary of the lesion site, and no astrocyte accumulation was observed in the implantation area at any time point. These findings indicate the feasibility of fabricating 3D spiral constructs using electrospun collagen fibers and demonstrated the potential of these scaffolds for SCI repair.

Introduction

Spinal cord injuries (SCIs) result in widespread loss of axonal connections and limited neuronal regeneration, which typically lead to functional impairment below the site of injury. The consequences are devastating, but unfortunately, effective methods of treatment are lacking. In general, a fluid-filled cavity typically forms at the injury site and becomes surrounded by a dense glial scar that is composed of astrocytes and connective tissue elements.[1] Astrocytes supply both structural and physiological support and respond rapidly for neural protection or healing after injury.[2,3] It was shown that reactive astrocytes play essential roles in preserving neural tissue and restricting inflammation after central nervous system (CNS) injury.[2] However, subsequent studies demonstrated that the inhibitory and nonpermissive nature of glial scar prevents successful axonal regeneration after SCI.[3,4] Besides being a mechanical barrier for axonal reconnections, the molecular composition of the glial scar and the inhibitory molecules secreted by astrocytes also contribute to regenerative failure.[2,5] Therefore, deeper understanding of astrocytes behaviors may contribute to optimal design strategies for SCI treatment.

To modulate the inhibitory environment after SCI, biomaterial scaffolds, particularly hydrogels, have been developed to bridge the injury gap. However, although a degree of

[1]School of Chemical and Biomedical Engineering, Nanyang Technological University, Singapore, Singapore.
[2]Department of Neurobiology and Anatomy, Drexel University College of Medicine, Philadelphia, Pennsylvania.
[3]Medical Engineering Program, Department of Mechanical Engineering, University of Hong Kong, Hong Kong Special Administrative Region, China.

cellular penetration is often observed, nerve regeneration remains sub-optimal.[6,7] One possible reason may be the isotropic nature of hydrogels. Since the spinal cord is comprised of highly oriented neural fibers, imparting topographical cues into scaffold designs for contact guidance may be beneficial. The observed directed axonal regeneration from rostral and caudal ends after SCI in the presence of implanted aligned collagen microfilaments supports this notion.[8,9]

Compared to microfilaments, nanofibers more closely mimic the size scale and architecture of the natural extracellular matrix and may elicit more physiologically relevant cellular phenotypes.[10,11] Electrospun nanofiber scaffolds, in particular, further permit control over nanofiber alignment to provide contact guidance to seeded cells.[12] In addition, it is easy to manipulate the macroscopic structure of these constructs for specific applications[13] and to encapsulate biomolecules[14–17] for a synergistic control over cell fate. To date, only few studies have demonstrated *in vivo* applications of electrospun synthetic nanofibers for nerve regeneration in the CNS.[18–20] Due to the lack of biofunctionality of synthetic polymers, further surface chemical modifications were often required to support neural cell function effectively.[18]

In this study, we evaluated the potential of using electrospun collagen nanofibers for SCI treatment. Collagen type I plays a role in neuronal pathfinding and growth cone guidance[21] and has been shown to provide a permissive environment for the regrowth of injured axons.[22] In our previous study, we demonstrated the feasibility of electrospinning collagen nanofibers by adopting acetic acid as the solvent to decrease protein denaturation. Furthermore, by incorporating a photochemical crosslinking process, the nanofiber architecture was stabilized for at least 21 days *in vitro*.[23] Here, we demonstrated the ability to form spiral conduits of electrospun collagen nanofibers and the feasibility of implanting these tubular constructs for the treatment of SCI.

Materials and Methods

Materials

Type I collagen was extracted from rat tails for electrospinning.[24] Ninety-nine percent acetic acid was purchased from Merck. Dulbecco's modified Eagle's medium (DMEM), minimum essential medium (MEM), neural basal medium, B27, L-glutamine, penicillin–streptomycin, 4′,6-diamidino-2-phenylindole (DAPI), antiglial fibrillary acidic protein (anti-*GFAP*), anti-*ED1*, anti-*Tuj1*, secondary antibodies, green-fluorescent calcein-acetoxymethyl ester (AM), and 5-ethynyl-2′-deoxyuridine (EdU) assay kits were purchased from Invitrogen. Fetal bovine serum (FBS) was purchased from Hyclone. Enzyme papain was from Worthington. Type I collagen solution was purchased from Roche Diagnostics for coating glass cover-slips as two-dimensional (2D) substrate control. Neurotrophin-3 (NT-3) was ordered from R&D System. All other chemicals and reagents were purchased from Sigma-Aldrich.

Fabrication of collagen nanofibers and nerve guide conduits

Collagen nanofibers were electrospun as described previously.[23] To obtain aligned and randomly oriented fibers, samples were collected on aluminum foils that were mounted on a grounded target that was rotating at 2500 and ~150 rpm respectively. Thereafter, all samples were photochemically crosslinked as described previously.[23] Spiral-shaped nerve guide conduits were then prepared by rolling the wet crosslinked scaffolds into tubes of 4–5 layers. After that, all samples were critical point dried (BAL-TEC CPD 030) and the underlying aluminum foil support was removed. For conduits with aligned fibers they were oriented longitudinally when placed into the injured spinal cord.

Evaluation of structure and appearance of nerve guide conduits

All samples were sputter-coated with platinum (JEOL, JFC-1600) for 90 s. Thereafter, the cross section of the conduit and fiber morphology was observed under the scanning electron microscope (JEOL, JSM-6390 LA) at an accelerating voltage of 10 kV.

Dorsal root ganglia culture and immunostaining

Dorsal root ganglias (DRGs) were dissected from E15-old embryos of Sprague Dawley rats under current Institutional Animal Care and Use Committee (IACUC) guidelines and placed in L15 medium. Before seeding the DRGs, crosslinked random and aligned collagen scaffolds were sterilized by ultraviolet (UV) irradiation for 15 min on each side and soaked in phosphate-buffered saline (PBS) at 37°C overnight to remove any chemical residues in the scaffolds. The isolated DRGs were then seeded onto sterilized collagen scaffolds in 24-well plates and cultured in neural basal medium containing 1% B27, 0.5 mM L-Glutamine, 1% penicillin–streptomycin, and 40 ng/mL NT-3. Glass coverslips coated with type I collagen were used as the 2D control. Type I collagen solution was added on UV-sterilized glass coverslips at a density of 5 μg/cm^2 and incubated at room temperature for 2 h. After that, the glass coverslips were washed with PBS for three times and air-dried for cell seeding.

At day 2, immunostaining was conducted to observe neurite outgrowth from DRGs that were fixed with 10% formalin and permeabilized with 0.1% Triton X-100 for 20 min. After thorough washes with PBS, the ganglia were blocked with 3% bovine serum albumin (BSA). Primary antibody against *Tuj-1* (1:500) was added and incubated with cells for 1 h at room temperature. After washing with PBS for three times, secondary antibody (Alexa Fluor 633, 1:500) was added. Cell nuclei were stained with DAPI (1:1000) and all images were taken under the confocal microscope (Zeiss, LSM 710).

Astrocyte cell culture

Primary cortical astrocytes were harvested from E18-old rat embryos under current IACUC guidelines following established protocol.[25] The cerebral cortices were isolated from the brains and the meninges were removed. The cortices were then digested with papain (25 U/mL). After digestion, cells were dissociated by filtering through a 70-μm cell strainer and collected by centrifugation. Cells were resuspended in MEM supplemented with 10% FBS, 2% glucose, and 1% penicillin–streptomycin in cell culture plate at a density of 2×10^5 cells/cm^2. Neuronal cells were removed by

constant agitation overnight. The culture medium was replaced every 2 days until the monolayer was obtained. Primary astrocytes with a purity of 99% were obtained based on this protocol. Thereafter, astrocytes were propagated in DMEM supplemented with 10% FBS and 1% penicillin–streptomycin. Cells of passage 4–9 were used in this study.

Before seeding the astrocytes, crosslinked collagen scaffolds were sterilized and soaked in PBS in 24-well plates to wash away any chemical residues. Thereafter, PBS was aspirated and astrocytes suspension were added onto the scaffolds at a density of 10^4 cells/well in 24-well plates ($n=3$). Glass cover slips coated with $5\,\mu g/cm^2$ of type I collagen as described above were used as the 2D substrate control. The culture medium was changed at day 3 for samples that were collected at day 7.

Evaluation of astrocyte morphology

At days 3 and 7, the effects of substrate topography on astrocyte morphology were evaluated by green-fluorescent calcein-AM staining following manufacturer's protocol. Cells were imaged under a fluorescent microscope (Olympus IX 71) at 10× magnification. To prevent bias, eight randomly chosen regions were imaged on each scaffold. Thereafter, morphometric measurements were carried out using ImageJ (NIH) and at least 100 cells were measured for each sample. The elongation factor (E) of astrocytes was calculated as follows: ([long axis/short axis] -1). E describes the extent to which the equimomental eclipse is lengthened or stretched out.[26,27] The value of E will reflect whether the astrocytes are elongated by the contact guidance with collagen fibers. Cell shape index, which was defined as cell perimeter^2/$4\pi\cdot$area, was calculated as a measurement of how circular or linear the cell was (where 1.0 indicates a rounded cell and a larger value implies a more dendritic cell shape).[28] Activated astrocytes are commonly recognized morphologically by converting from flat, polygonal cells to contracted and highly branched cells. Cell shape index, which is also named as dendritic index, may reflect the activated state of astrocytes.[29]

Evaluation of astrocyte proliferation

Astrocyte proliferation in response to substrate topography was quantified by measuring DNA synthesis using EdU incorporation assay following manufacturer's protocol. At days 3 and 7, EdU was added into the cell culture medium for 18 h. Thereafter, all samples were fixed in 10% formalin and permeabilized with 0.1% Triton X-100 for 20 min. For EdU detection, the click-it reaction was performed according to the manufacturer's instructions. To calculate EdU incorporation rate, 9 images were taken at different regions and at least 200 cells were counted for each sample.

Evaluation of GFAP expression in astrocytes

Immunostaining was conducted at days 3 and 7 to observe the expression levels of *GFAP* in astrocytes seeded on different substrates. Scaffolds seeded with cells were fixed and permeabilized as the protocol described previously. After thorough washes with PBS, the scaffolds were blocked with 3% BSA. Primary antibodies against *GFAP* (1:500) were added and incubated with cells for 1 h at room temperature. After washing with PBS for three times, secondary antibody (Alexa Fluor 633, 1:500) was added and cell nuclei were labeled with DAPI (1:1000). All images were taken by using the same settings under a Zeiss confocal microscope (LSM 710). To calculate fluorescence intensity of *GFAP*, 24 separate images were taken at different regions and at least 100 cells were analyzed. The fluorescence intensity of *GFAP* was quantified by a modified protocol.[30] Briefly, after converting to eight-bit images, the shape of each cell was outlined and single-cell fluorescent intensity was measured by ImageJ.

In vivo *studies: hemisection SCI model*

The care and use of laboratory animals and all surgical procedures followed the guidelines by the National Institute of Health and Drexel University College of Medicine IACUC. Eight adult female Sprague Dawley rats (225–250 g) were anesthetized under isoflurane delivered at a flow rate of 0.2 L/min. A cervical level 3 (C3) complete unilateral hemisection (Hx) lesion cavity of 2.5 mm in length was then created by aspiration. Thereafter, UV-sterilized collagen tubes (2.5 mm in length, 2 mm in diameter) were implanted into the injury site. The animals were implanted with either random ($n=3$) or aligned collagen scaffolds ($n=5$). For all samples, the longitudinal axis of the conduit was parallel to the long axis of the spinal cord.

To evaluate the *in vivo* stability of the collagen scaffolds, 10- and 30-day time points were chosen. At day 10, three animals (random, $n=1$; aligned, $n=2$) were euthanized with an overdose of Euthasol (390 mg/kg pentobarbital and 50 mg/kg phenytoin, intraperitoneal) and perfused transcardially with 4% paraformaldehyde in 0.1 M Sorenson's phosphate buffer. The remaining animals (random, $n=2$; aligned, $n=3$) were sacrificed and perfused by the same way at day 30. The C3 spinal cord surrounding the lesion site was then removed, postfixed at 4°C for 4 h, and submersed in 20% sucrose for 24 h at 4°C. Cryostat sections at 25 μm in both transverse and longitudinal planes were prepared for immunofluorescent staining.

Immunofluorescent staining of spinal cord sections

Slides were stored at −80°C until immunostaining was performed. Sections were incubated in phosphate buffered 4% paraformaldehyde for 15 min and then washed with 0.1 M Sorenson's phosphate buffer before being permeabilized in Triton X-100 PBS (T-PBS) for 15 min. After thorough washes in PBS, the sections were blocked for nonspecific reactivity with normal goat serum/T-PBS (1:20) for 15 min. Primary antibodies were applied to the sections and incubated overnight at room temperature. The primary antibodies were against the following: *ED1* (recognizing marcrophages, 1:1000), Neurofilament (recognizing neurons, 1:400), and *GFAP* (recognizing astrocytes, 1: 1000). *GFAP* and *ED1* were double labeled on slides. After washing with Sorenson's phosphate buffer, slides labeled for GFAP and neurofilament were incubated with Alexa fluor 488 goat anti-rabbilt antibody (at 1:1000 dilution). Slides labeled with *ED1* were incubated Texas Red rabbit anti-mouse antibody (at 1:1000 dilution) for 90 min. All slides were coverslipped with fluoromount mounting medium and examined under the confocal microscope at 10× and 20× magnifications.

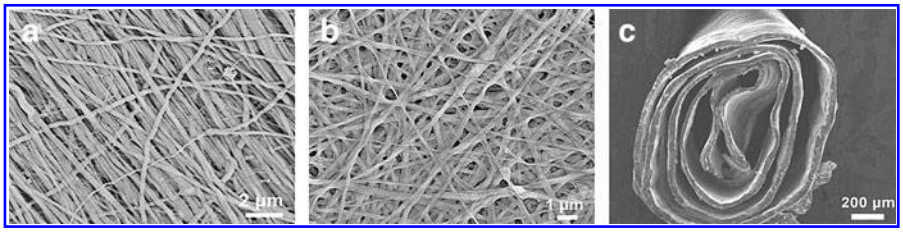

FIG. 1. SEM images of electrospun collagen aligned fibers **(a)**, random fibers **(b)**, and cross section of collagen nerve guide conduit composed of aligned fibers **(c)**. SEM, scanning electron microscopy.

To examine the *in vivo* stability of collagen scaffolds and the extent of tissue–implant integration, Masson's trichrome staining was conducted (Biopolis Shared Facilities–Histology, Biomedical Sciences Institutes, Singapore). Thereafter, all samples were examined using a light microscope (Olympus, IX71).

Statistic analysis

All data presented in this study are expressed as mean ± standard error (SE) of mean. For the analyses of elongation factor and cell shape index, Mann–Whitney *U* test was used. One-way analysis of variance was used to analyze EdU incorporation rate of astrocytes and the fluorescent intensity of *GFAP* expressed on random, aligned collagen nanofibers and collagen-coated glass cover slips. Independent-samples *t*-test (SPSS Statistics 17.0) was used for comparing *GFAP* intensity differences between day 3 and 7 on different substrates. Error bar represents the SE of the mean.

Results

Morphology and appearance of electrospun collagen fibers and nerve guide conduits

Figure 1a and b illustrate the architecture of photochemically crosslinked electrospun collagen scaffolds that are comprised of aligned and randomly oriented nanofibers, respectively. Uniform nanofibers with an average diameter of 208.2 ± 90.4 nm were obtained in both conditions. Regardless of fiber orientation, all collagen conduits looked similar macroscopically, and as shown in Figure 1c, the cross section of the nerve guide conduits revealed a spiral structure that comprised of 4–5 layers of nanofiber scaffold.

DRG neurite outgrowth

As shown in Figure 2a, the neurite outgrowth from DRG explants followed the orientation of aligned collagen fibers. In contrast, neurites emanated radially from DRG tissues that were cultured on randomly oriented collagen fibers and collagen-coated glass cover slips, generating a rounded appearance (Fig. 2b, c).

Astrocytes morphology

As shown in Figure 3a, astrocytes responded to the aligned nanofiber architecture and exhibited elongated morphology. In contrast, astrocytes spread and adopted nonspecific orientations on randomly oriented fibers and collagen-coated glass cover slips (Fig. 3b, c). Correspondingly, the elongation factor and cell shape index of astrocytes were significantly higher on aligned fibers, while no significant difference was found between randomly oriented fibers and 2D controls (Fig. 3d, e).

Astrocytes proliferation

On day 3, the proliferation of astrocytes was significantly lower on collagen nanofibers than on 2D controls (Fig. 4, $p < 0.05$). No significant difference was detected in response to fiber orientation. On day 7, no EdU incorporation was found in astrocytes that were seeded on collagen substrates. On the other hand, EdU incorporation decreased to 18.9% ± 8.1% on collagen-coated cover slips ($p < 0.01$).

Astrocytes GFAP expression

As indicated in Figure 5, *GFAP* signal intensity was significantly higher in astrocytes that were cultured on 2D controls than collagen nanofiber substrates on days 3 and 7 ($p < 0.05$ and $p < 0.01$, respectively; Fig. 5g). However, there was no significant difference between randomly oriented and aligned fibers. On day 7, the signal intensity decreased significantly on collagen scaffolds ($p < 0.05$), while no significant alteration was found on collagen-coated cover slips.

Collagen scaffold in vivo *stability and biocompatibility*

Figure 6 illustrates the spinal cord sections that were stained with Masson's trichrome, where blue staining indicates collagenous material. On day 10, the collagen walls that

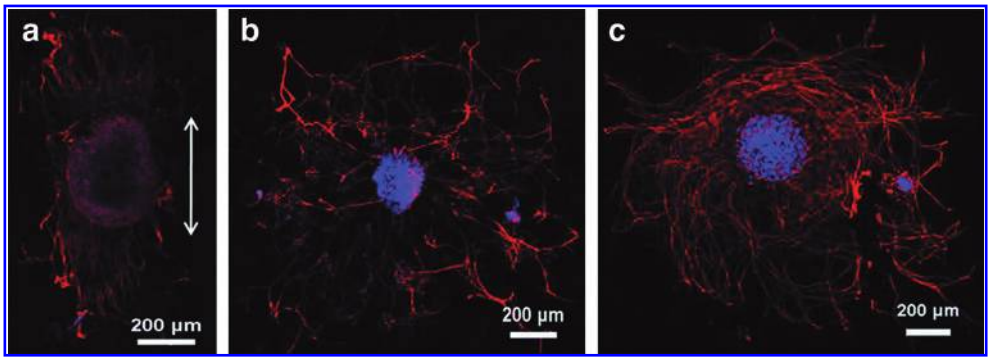

FIG. 2. Tuj-1 staining of DRG explants seeded on aligned collagen fibers **(a)**, random collagen fibers **(b)**, and collagen-coated glass cover slips **(c)**. White arrow indicates the alignment of collagen fibers. Red, Tuj-1; blue, DAPI. DRG, dorsal root ganglia; DAPI, 4′,6-diamidino-2-phenylindole. Color images available online at www.liebertonline.com/tea

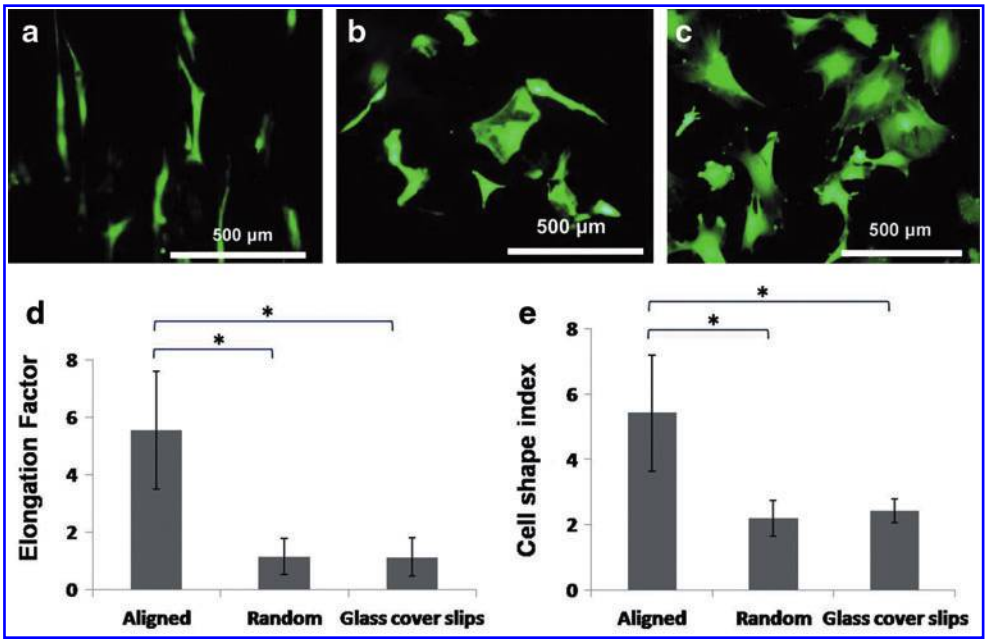

FIG. 3. Calcein-AM staining of astrocytes seeded on aligned collagen fibers **(a)**, random collagen fibers **(b)**, and collagen-coated glass cover slips **(c)**. Elongation factor **(d)** and cell shape index **(e)** of astrocytes seeded on different substrates. $n = 3$, mean ± SE (*$p < 0.01$, Mann–Whitney U test). AM, acetoxymethyl ester; SE, standard error. Color images available online at www.liebertonline.com/tea

made up the spiral architecture remained intact as shown in the sagittal sections of the tissues (Fig. 6a). As indicated in Figure 6c, the spiral configuration of the collagen constructs was retained. In general, the longitudinal axes of the spiral conduits remained parallel to the spinal cords, demonstrating the structural stability of the conduits. However, the orientation of the collagen walls was not strictly uniform due to artificial sectioning defects. Significant cell penetration was found within the walls and the interior sections of the conduits regardless of fiber orientation (Fig. 6b, d). In general, no significant difference was observed in host–implant integration in response to fiber orientation and no cystic cavity was observed in any animals.

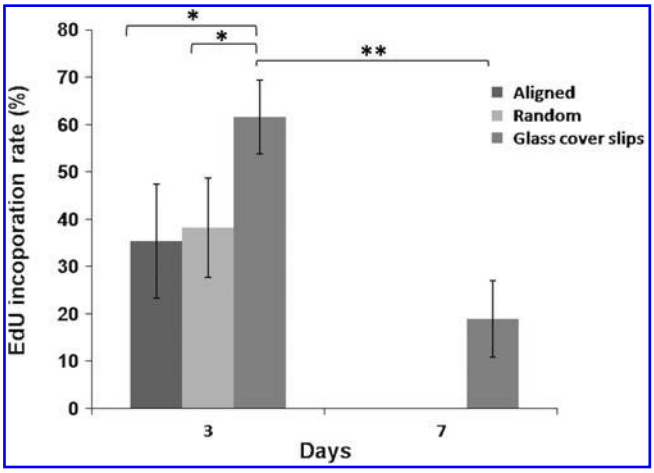

FIG. 4. EdU incorporation rate of astrocytes seeded on aligned and randomly oriented collagen fibers, and collagen-coated glass cover slips. $n = 3$, mean ± SE (*$p < 0.05$, ANOVA; **$p < 0.01$, independent t-test). EdU, 5-ethynyl-2′-deoxyuridine; ANOVA, analysis of variance.

On day 30, Masson's trichrome staining showed decreased presence of cells within all implants, suggesting a possible reduction in the acute inflammatory response (Fig. 6g, h).

Figure 6e and f reveals the sagittal sections of the spinal cord. On day 30, the walls of aligned collagen nanofiber scaffolds remained visible. On the other hand, constructs that comprised of randomly oriented fibers degraded and no collagen remnant was observed in the cross sections of the tissues (Fig. 6g, h).

Immunofluorescent staining for inflammatory response, astrocytes accumulation, and neural fiber sprouting

Figure 7 illustrates the immunofluorescent images of the spinal cord sections. As shown in Figure 7a, d, g, and j, *ED1* immunolabeling was used to examine the macrophage responses, which were stained as dot-like structures that accumulated at the boundary of the lesion sites. Crosslinked collagen scaffolds demonstrated strong autofluorescence at a wavelength of 520–570 nm due to the photo initiator (rose bengal) that was added for crosslinking[23] and appeared as blocky patterns. On day 10, strong *ED1* signals were detected in all animals, suggesting strong inflammatory response. However, no significant difference was observed between randomly oriented and aligned nanofiber constructs (Fig. 7a, d). On day 30, the *ED1* signal intensity decreased significantly in all samples. In animals that received randomly oriented nanofiber scaffolds, a few macrophages were observed at the border of the lesion areas (Fig. 7j), while no *ED1* signal was observed in animals that received aligned nanofiber substrates (Fig. 7g).

At both time points, *GFAP* was not detected within the scaffold in any of the animals. In contrast, reactive astrocytes stained by *GFAP* were present at the borders of the lesion areas (Fig. 7b, e, h, and k).

When treated with collagen scaffolds for 10 days, some neurofilament sprouting was observed at the site of

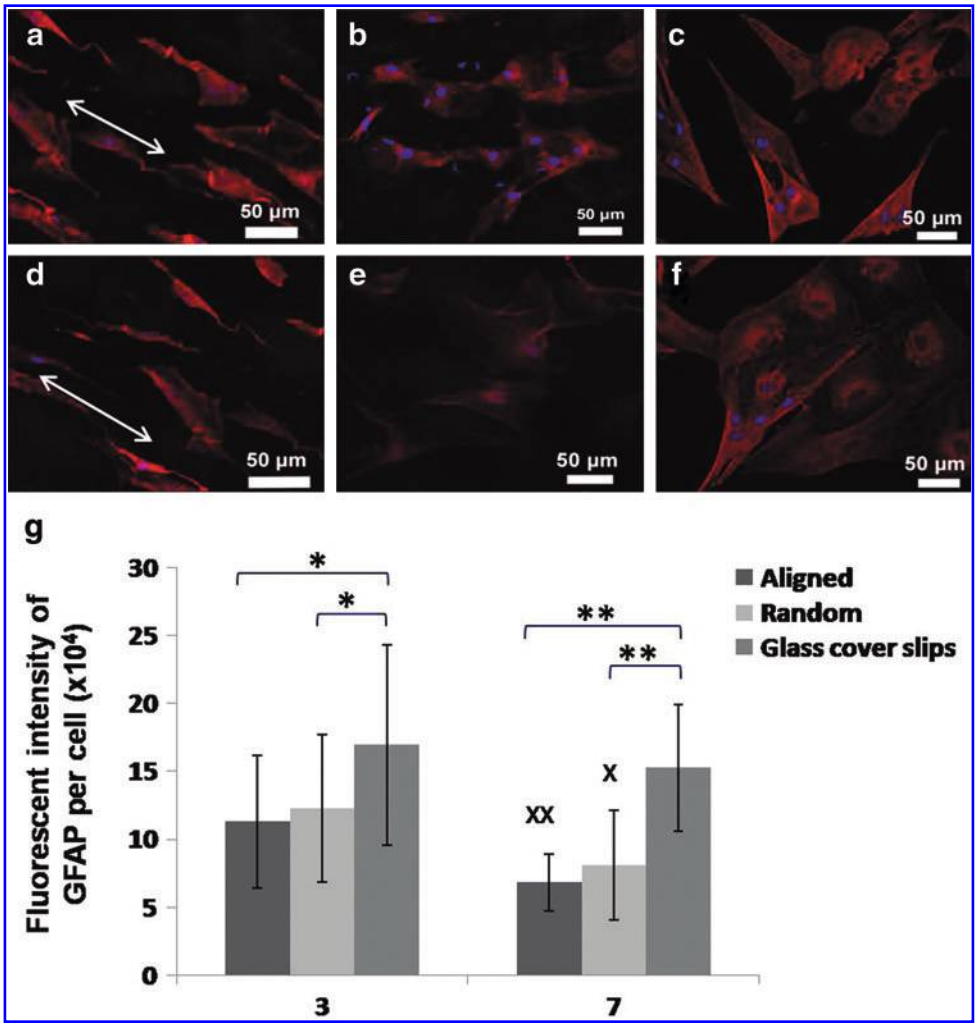

FIG. 5. GFAP staining of astrocytes seeded on aligned collagen fibers **(a, d)**, random collagen fibers **(b, e)**, and collagen-coated glass cover slips **(c, f)** for 3 days **(a–c)** and 7 days **(d–f)**. White arrows indicate the alignment of collagen fibers. Red, GFAP; blue, DAPI. GFAP fluorescent intensity per cell **(g)**. $n=3$, mean ± SE (*$p<0.05$, **$p<0.01$, ANOVA; X denotes $p<0.05$, XX denotes $p<0.01$ vs. day 3, independent t-test). GFAP, glial fibrillary acidic protein. Color images available online at www.liebertonline.com/tea

injury regardless of nanofiber orientation (Fig. 7c, f). Neurofilament was detected at the rostral and caudal ends of the aligned samples. However, the orientation of regenerated axons in response to fiber alignment was not obvious at both time points. In the cross-sectional images of constructs that comprised of randomly oriented fibers, neurofilament was detected mainly around the outer regions of the implants and limited amount of neural fibers were observed at the middle points of the conduits (Fig. 7f).

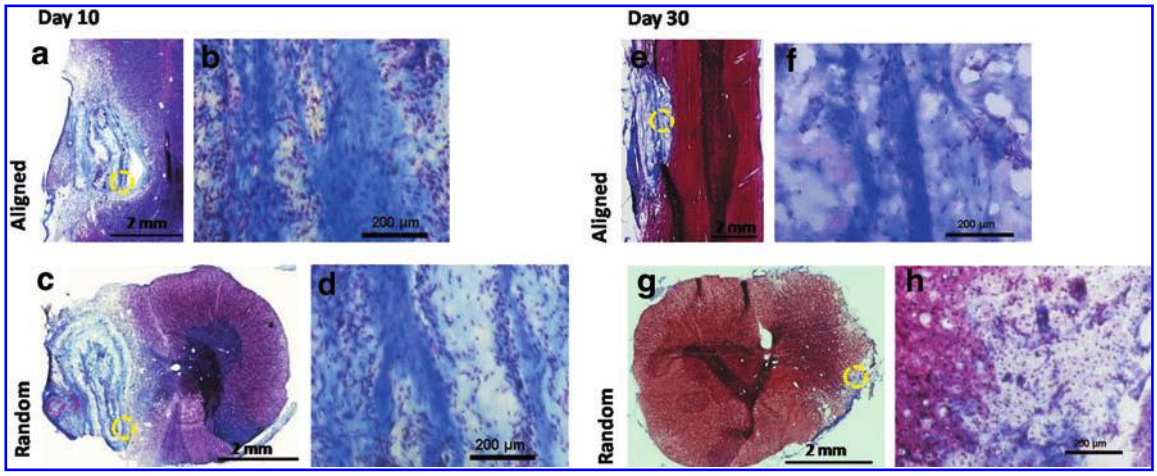

FIG. 6. Masson's trichrome staining of spinal cord implanted with collagen scaffolds for 10 days **(a–d)** and 30 days **(e–h)**. Images of spinal cord implanted with aligned scaffolds **(a, b, e, f)** in a longitudinal plane and random scaffold in a transverse plane **(c, d, g, h)**. Higher magnification (20×) images of the area indicated by dash circles show cell penetration into scaffolds **(b, d, f, h)**. Color images available online at www.liebertonline.com/tea

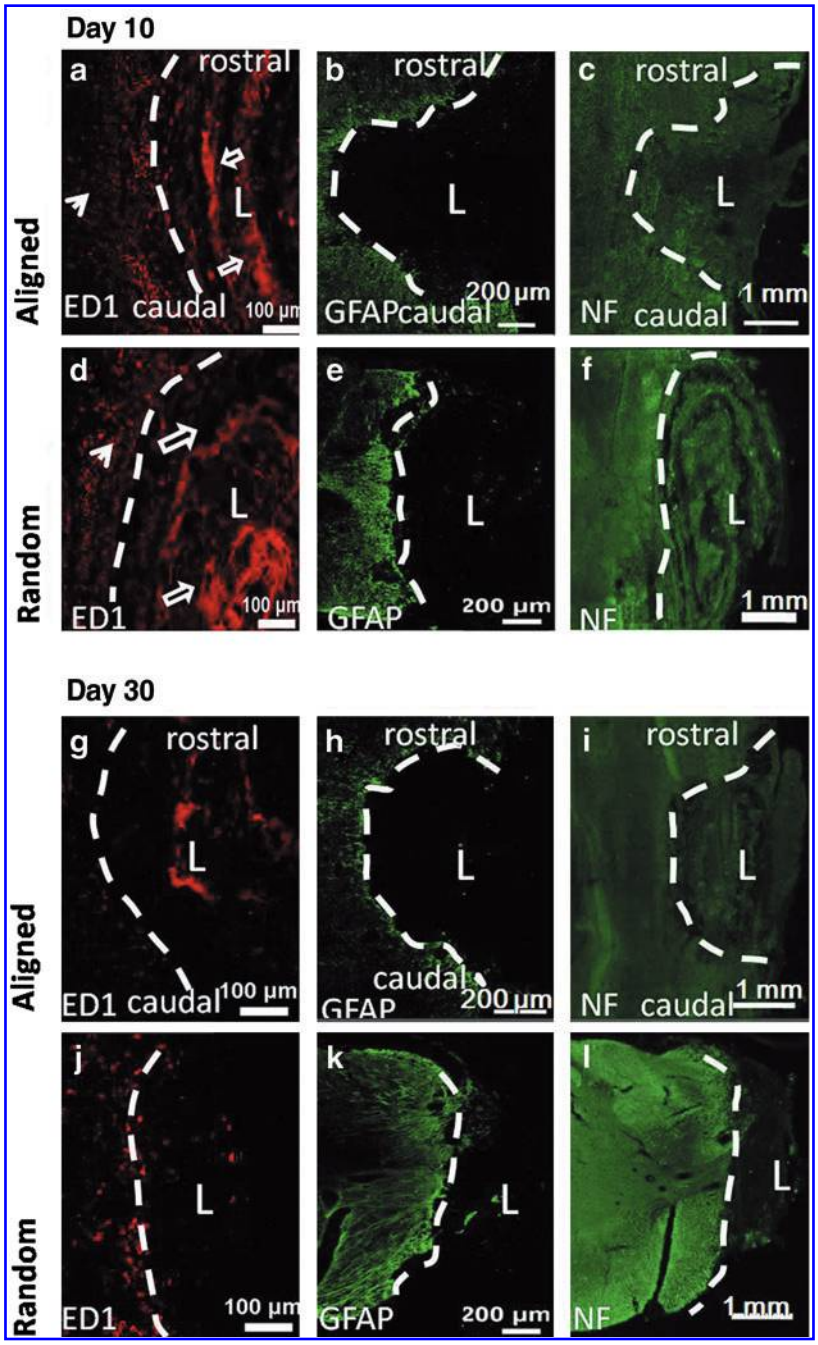

FIG. 7. Immunofluorescent images of spinal cord sections implanted with collagen scaffolds for 10 days **(a–f)** and 30 days **(g–l)**. Spinal cords were implanted with collagen spiral conduits composing of aligned fibers in a longitudinal plane **(a–c, g–i)** and randomly oriented fibers in a transverse plane **(d–f, j–l)**. White dash line indicates lesion border and "L" indicates lesion area. Spinal cord sections were stained with ED1 **(a, d, g, j)**, GFAP **(b, e, h, k)**, and NF **(c, f, i, l)**. ED1-positive macrophages were stained as red dots (filled arrows). Collagen scaffolds demonstrated strong autofluorescence and appeared as blocky patterns (open arrows). GFAP, green; ED1, red; NF, green. Color images available online at www.liebertonline.com/tea

Discussion

Current SCI treatment methods remain limited due in part to the complex inhibitory microenvironment after injuries. An ideal tissue construct for SCI treatment should help lessen glial scar formation and support axon extensions. Additionally, the scaffold should be able to direct regenerating axons across the injury site to restore functional connections. Currently, hydrogels are often used for scaffold implantation treatments in SCI models.[31–33] Although enhanced structural recovery has been reported as compared to treating the injury without any scaffold, nerve regeneration remains suboptimal. A possible reason may be the isotropic nature of hydrogels, which lacks topographical signals for cellular contact guidance.[6,7] In contrast, nanofibers provide biomimicking signals and result in attraction of more physiologically relevant cellular phenotypes.[34–36] Applied to neural tissue engineering, nanofiber topography, particularly the aligned fibers, can enhance Schwann cell maturation[37,38] and direct neurite outgrowth.[39,40]

Plain electrospun collagen nanofibers supported neurite outgrowth from DRGs (Fig. 2). Presented in aligned format, alignment of neurite outgrowth was observed. This demonstrated the contact guidance provided by aligned nanofibers, which is consistent with the literature.[39] In addition, we evaluated *in vitro* glial cell interactions with nanofibers. Although equally important in the nerve regeneration process, glial cell behavior is less extensively evaluated in neural

tissue engineering studies. In this work, we focused on astrocyte behavior since they are the major contributors to glial scar formation upon activation after an injury to the CNS.[41]

When cultured on randomly oriented fibers, the cell shape index of astrocytes was similar to that on collagen-coated cover slips. Although cell shape index on aligned collagen fibers was significantly higher, astrocytes did not demonstrate truly ramified morphological changes. The higher cell shape index was likely caused by the elongated morphology in response to aligned nanofibers instead of enhanced cellular activation. These results suggested that the extent of astrocytes activation was not enhanced by nanofiber topography in comparison to 2D controls. This was also substantiated by *GFAP* expression analysis.

Activated astrocytes are usually characterized by hypertrophy, proliferation, and increased *GFAP* expression.[42,43] However, we observed decreased astrocyte proliferation and *GFAP* expression on electrospun nanofibers versus 2D collagen coating. Combining our observation with prior studies that showed alterations in astrocyte morphology and migration and decreased proliferation in response to electrospun nanofibers,[39,44,45] we find that the topography of nanofibers may have altered cell attachment, thereby changing intracellular signaling pathways that were connected with the control of cell behavior and suppressed the expression of *GFAP*. Furthermore, no obvious differences in *GFAP* expression were observed in astrocytes in response to nanofiber orientation (Fig. 5). This result is consistent with the observations by East *et al.*, where astrocytes expressed similar levels of *GFAP* regardless of fiber alignment on collagen gels.[46] Matrix stiffness affects cell proliferation, protein production, cell motility, and cell fate.[47,48] Decreased astrocytes adhesion on soft gels were observed due either to migration off the soft gel or to detachment.[48] It is possible that the in our study, matrix stiffness overrides the topographical cues and became the predominant factor manipulating astrocyte cell fate. Therefore, no significant difference in astrocytes proliferation rate and *GFAP* expression was observed between aligned and randomly oriented fibers. Further analyses on cell signaling pathways involved in matrix topography and stiffness sensing by astrocytes would provide useful information on these areas. Nonetheless, taken together, the results suggested that nanofibers may decrease the extent of astrocyte involvement post-SCI. Coupled with the ability to support and direct neurite outgrowth, electrospun collagen scaffolds may be more favorable than collagen introduced in 2D format for SCI repair.

To explore the feasibility of implanting electrospun collagen spiral nerve conduits into the spinal cord and to evaluate the *in vivo* structural stability of the constructs, a short-term acute hemi-section SCI model was chosen. By this injury, unilateral ascending sensory axons and descending motor axons were damaged. As a preliminary study, only a total of 8 rats were used. The 10- and 30-day endpoints were chosen based on previous *in vitro* stability studies that indicated ~50% and 70% scaffold mass loss by days 7 and 15, respectively.[23] In addition, 30 days are thought to be sufficient for significant neural regeneration to occur for meaningful analyses of structural recovery.[49] As revealed by Masson's trichrome staining, the spiral structures of all collagen nerve conduits were retained after implantation. This indicated the feasibility of fabricating and implanting such spiral constructs. At day 30, conduits that comprised of randomly oriented fibers were almost completely degraded, while the structure of aligned collagen tubes remained visible. Randomly oriented nanofibers significantly enhance initial monocyte adhesion as compared to aligned fibers.[50] This may partially explain the faster degradation rate of randomly oriented collagen fiber spiral conduits. Further detailed quantitative analyses on the extent of macrophage invasion with respect to conduit topography using larger sample sizes may provide useful insights.

Significant cell penetration into all collagen scaffolds was observed as early as day 10, regardless of nanofiber orientation. In contrast, cellular infiltration rarely occurred in randomly oriented electrospun synthetic polymer fibers.[50] This difference may be attributed to the more compliant nature of collagen and its faster *in vivo* degradation rate.[51,52] The migration of support cells into the injured site is essential to induce or support tissue regeneration by providing an extracellular milieu.[31] Therefore, electrospun collagen fibers may be indicated as a preferential material for SCI treatment.

The significant decrease in cell density and *ED1*-positive cells by day 30 suggested that there was a reduction in acute inflammatory response and that the electrospun collagen scaffolds were biocompatible. Dense glial scar often forms after SCI and hinders the regeneration of axons.[53] However, no obvious accumulation of *GFAP*-positive cells were detected at the interface of the lesion site and the scaffolds, indicating a possible decrease in astroglial scar formation in the presence of collagen implants. One possible reason may be the suppressive nature of collagen nanofibers over astrocyte proliferation seen *in vitro*.

When treated with collagen, some neural fiber sprouting was observed in both groups as early as day 10. However, the organization and orientation of regenerated axons in response to nanofiber alignment were not obvious at either time point. Markedly linear axonal regeneration was observed inside aligned electrospun conduits using microfibers with diameter of 1.2–1.6 μm after 2-week implantation in a complete transection SCI model.[20] In addition, the influences of fiber diameter on axonal outgrowth have been observed by *in vitro* studies and larger diameter fibers (~1.3 μm) elicited longer neurite outgrowth than smaller diameter fibers (~290 nm).[54] Taken together, these results suggested that larger fiber diameter may have more significant influence on axonal outgrowth. The diameter of collagen fibers used in this study was 208.2 ± 90.4 nm. This smaller diameter could be a possible reason for the insignificant difference in orientation of regenerated neural fibers *in vivo* in response to fiber orientation. However, the exact effect of fiber diameter on the guidance of axonal outgrowth *in vivo* needs to be elucidated in further works. In addition, due to the limited sample size in this study, the exact trend of neural fiber orientation in response to fiber alignment may not be elicited. Future works involving larger number of animals may help shed light in this area. Electrospun nanofibers may be easily functionalized through protein incorporation to provide synergistic topographical and biochemical signaling to enhance nerve regeneration.[15] Further works involving neurotrophin incorporation within collagen electrospun scaffolds may also be conducted for enhanced nerve regeneration in SCI.

Conclusions

This study investigated the feasibility of using collagen electrospun fibers for SCI treatment. Collagen nanofibers suppressed astrocyte proliferation and *GFAP* expression, and supported and directed DRG neurite outgrowth *in vitro*. Preliminary *in vivo* studies showed that collagen electrospun fibers diminished astrocyte accumulation at the lesion site, provided a permissive environment for cellular infiltration and supported neural fiber sprouting. These findings clearly demonstrate the potential of electrospun collagen scaffolds for SCI repair.

Acknowledgments

This work was partially supported by the National Medical Research Council (NMRC) Exploratory/Development Grant (NMRC/EDG/0027/2008) and the A*Star BMRC Grant (07/1/22/19/519), Singapore. The animal experiment conducted in Drexel University was supported by National Institutes of Health (US) and NINDS NS26380 (JDH) granted to Dr. John D. Houle. The authors thank Dr. Eyleen Goh for her generous supply of primary astrocytes.

Disclosure Statement

No competing financial interests exist.

References

1. Willerth, S.M., and Sakiyama-Elbert, S.E. Approaches to neural tissue engineering using scaffolds for drug delivery. Adv Drug Deliver Rev **59,** 325, 2007.
2. Fitch, M.T., Doller, C., Combs, C.K., Landreth, G.E., and Silver, J. Cellular and molecular mechanisms of glial scarring and progressive cavitation: *in vivo* and *in vitro* analysis of inflammation-induced secondary injury after CNS trauma. J Neurosci **19,** 8182, 1999.
3. Sliver J., and Miller, J.H. Regeneration beyond the glial scar. Nat Rev Neurosci **5,** 146, 2004.
4. Grandpre, T., and Strittmatter, S.M. Nogo: A molecular determinant of axonal growth and regeneration. Neuroscientist **7,** 377, 2001.
5. Busch, S.A., and Silver, J. The role of extracellular matrix in CNS regeneration. Curr Opin Neurobiol **17,** 120, 2007.
6. Taylor, S.J., McDonald, J.W., and Sakiyama-Elbert, S.E. Controlled release of neurotrophin-3 from fibrin gels for spinal cord injury. J Control Release **98,** 281, 2004.
7. Taylor, S.J., and Sakiyama-Elbert, S.E. Effect of controlled delivery of neurotrophin-3 from fibrin on spinal cord injury in a long term model. J Control Release **116,** 204, 2006.
8. Yoshii, S., Oka, M., Shima, M., Akagi, M., and Taniguchi, A. Bridging a spinal cord defect using collagen filament. Spine **28,** 2346, 2003.
9. Yoshii, S., Ito, S., Shima, M., Taniguchi, A., and Akagi, M. Functional restoration of rabbit spinal cord using collagen-filament scaffold. J Tissue Eng Regen Med **3,** 19, 2009.
10. Christopherson, G.T., Song, H., and Mao, H.Q. The influence of fiber diameter of electrospun substrates on neural stem cell differentiation and proliferation. Biomaterials **30,** 556, 2009.
11. Noriega, S.E., Hasanova, G.I., Schneider, M.J., Larsen, G.F., and Subramanian, A. Effect of fiber diameter on the spreading, proliferation and differentiation of chondrocytes on electrospun chitosan matrices. Cells Tissues Organs 2011 [Epub ahead of print]; DOI: 10.1159/000325144.
12. Kempf, M., Miyamura, Y., Liu, P.-Y., Chen, A.C.H., Nakamura, H., Shimizu, H., Tabata, Y., Kimble, R.M., and McMillan, J.R. A denatured collagen microfiber scaffold seeded with human fibroblasts and keratinocytes for skin grafting. Biomaterials **32,** 4782, 2011.
13. Sell, S.A., Wolfe, P.S., Garg, K., McCool, J.M., Rodriguez, I.A., and Bowlin, G.L. The use of natural polymers in tissue engineering: a focus on electrospun extracellular matrix analogues. Polymers **2,** 522, 2010.
14. Chew, S.Y., Wen, J., Yim, E.K.F., and Leong, K.W. Sustained release of proteins from electrospun biodegradable fibers. Biomacromolecules **6,** 2017, 2005.
15. Chew, S.Y., Mi, R., Hoke, A., and Leong, K.W. Aligned protein–polymer composite fibers enhance nerve regeneration: a potential tissue-engineering platform. Adv Funct Mate **17,** 1288, 2007.
16. Cao, H., Jiang, X., Chai, C., and Chew, S.Y. RNA interference by nanofiber-based siRNA delivery system. J Control Release **144,** 203, 2011.
17. Rujitanaroj, P.-O., Wang, Y.-C., Wang, J., and Chew, S.Y. Nanofiber-mediated controlled release of siRNA complexes for long term gene-silencing applications. Biomaterials **32,** 5915, 2011.
18. Gelain, F., Antonini, S.P., Cunha, C., Donega, M., Lowery, J., Taraballi, F., Cerri, G., Montagna, M., Baldissera, F. and Vescovi, A. Transplantation of nanostructured composite scaffolds results in the regeneration of chronically injured spinal cords. ACS Nano **5,** 227, 2011.
19. Meiners, S., Ahmed, I., Ponery, A.S., Amor, N., Harris, S.L., Ayres, V., Fan, Y., Chen, Q., Delgado-Rivera, R., and Babu, A.N. Engineering electrospun nanofibrillar surfaces for spinal cord repair: a discussion. Polym Int **56,** 1340, 2007.
20. Hurtado, A., Cregg, J.M., Wang, H.B., Wendell, D.F., Oudega, M., Gilbert, R.M., and McDonald, J.W. Robust CNS regeneration after complete spinal cord transection using aligned poly-L-lactic acid microfibers. Biomaterials **32,** 6068, 2011.
21. Turner, D.C., Flier, L.A., and Carbonetto, S. Identification of a cell-surface protein involved in PC12 cell-substratum adhesion and neurite outgrowth on laminin and collagen. J Neurosci **9,** 3287, 1989.
22. Condic, M.L. Adult neuronal regeneration induced by transgenic integrin expression. J Neurosci **21,** 4782, 2001.
23. Liu, T., Teng, W.K., Chan, B.P., and Chew, S.Y. Photochemical crosslinked electrospun collagen nanofibers: synthesis, characterization and neural stem cell interactions. J Biomed Mater Res A **95A,** 276, 2010.
24. Rajan, N., Habermehl, J., Cote, M.-F., Doillon, C.J., and Mantovani, D. Preparation of ready-to-use, storable and reconstituted type I collagen from rat tail tendon for tissue engineering applications. Nat Protoc **1,** 2753, 2007.
25. Schwartz, J.P., and Wilson, D.J. Preparation and characterization of type 1 astrocytes cultured from adult rat cortex, cerebellum, and striatum. Glia **5,** 75, 1992.
26. Yim, E.K.F., Pang, S.W., and Leong, K.W. Synthetic nanostructures inducing differentiation of human mesenchymal stem cells into neuronal lineage. Exp Cell Res **313,** 1820, 2007.
27. Andersson, A.-S., Bäckhed, F., von Euler, A., Richter-Dahlfors, A., Sutherland, D., and Kasemo, B. Nanoscale

features influence epithelial cell morphology and cytokine production. Biomaterials **24,** 3427, 2003.
28. Miron-Mendoza, M., Seemann, J., and Grinnell, F. The differential regulation of cell motile activity through matrix stiffness and porosity in three dimensional collagen matrices. Biomaterials **31,** 6425, 2010.
29. Liu, W., Shafit-Zagardo, B., Aquino, D.A., Zhao, M.-L., Dickson, D.W., Brosnan, C.F., and Lee, S.C. Cytoskeletal alterations in human fetal astrocytes induced by interleukin-1β. J Neurochem **63,** 1625, 1994.
30. Dieterich, D.C., Hodas, J.L., Gouzer, G., Shadrin, I.Y., Ngo, J.T., Triller, A., Tirrel, D.A., and Schuman, E.M. *In situ* visualization and dynamics of newly synthesized proteins in rat hippocampal neurons. Nat Neurosci **13,** 897, 2010.
31. Johnson, P.J., Parker, S.R., and Sakiyama-Elbert, S.E. Fibrin-based tissue engineering scaffolds enhance neural fiber sprouting and delay the accumulation of reactive astrocytes at the lesion in a subacute model of spinal cord injury. J Biomed Mater Res A **92,** 152, 2010.
32. Nomura, H., Katayama, Y.M., Shoichet, M.S., and Tator, C.H. Complete spinal cord transection treated by implantation of a reinforced synthetic hydrogel channel results in syringomyelia and caudal migration of the rostral stump. Neurosurgery **59,** 183, 2006.
33. Tsai, E.C., Dalton, P.D., Shoichet, M.S., and Tator, C.H. Matrix inclusion within synthetic hydrogel guidance channels improves specific supraspinal and local axonal regeneration after complete spinal cord transection. Biomaterials **27,** 519, 2006.
34. Berrier, A.L., and Yamada, K.M. Cell–matrix adhesion. J Cell Physiol **213,** 565, 2007.
35. Green, J.A., and Yamada, K.M. Three-dimensional microenvironments modulate fibroblast signaling responses. Adv Drug Deliver Rev **59,** 1293, 2007.
36. Delgado-Rivera, R., Harris, S.L., Ahmed, I., Babu, A.N., Patel, R.P., Ayres, V., Flowers, D., and Meiners, S. Increased FGF-2 secretion and ability to support neurite outgrowth by astrocytes cultured on polyamide nanofibrillar matrices. Matrix Biol **28,** 137, 2009.
37. Chew, S.Y., Mi, R., Hoke, A., and Leong, K.W. The effect of the alignment of electrospun fibrous scaffolds on Schwann cell maturation. Biomaterials **29,** 653, 2008.
38. Jiang, X., Lim, S.H., Mao, H.-Q., and Chew, S.Y. Current applications and future perspectives of artificial nerve conduits. Exp Neurol **223,** 86, 2010.
39. Schnell, E., Klinkhammer, K., Balzer, S., Brook, G., Klee, D., Dalton, P., and Mey, J. Guidance of glial cell migration and axonal growth on electrospun nanofibers of poly-[epsilon]-caprolactone and a collagen/poly-[epsilon]-caprolactone blend. Biomaterials **28,** 3012, 2007.
40. Cao, H., Liu, T., and Chew, S.Y. The application of nanofibrous scaffolds in neural tissue engineering. Adv Drug Deliver Rev **61,** 1055, 2009.
41. McKeon, R.J., Schreiber, R.C., Rudge, J.S., and Silver, J. Reduction of neurite outgrowth in a model of glial scarring following CNS injury is correlated with the expression of inhibitory molecules on reactive astrocytes. J Neurosci **11,** 3398, 1991.
42. Ridet, J.-L., Privat, A., and Sudarshan, K.M. Reactive astrocytes, their roles in CNS injury, and repair mechanisms. Adv Str Bio **6,** 147, 2000.
43. Ferraguti, F., Corti, C., Valerio, E., Mion, S., and Xuereb, J. Activated astrocytes in areas of kainate-induced neuronal injury upregulate the expression of the metabotropic glutamate receptors 2/3 and 5. Exp Brain Res **137,** 1, 2001.
44. Gerardo-Nava, J., Fuhrmann, T., Klinkhammer, K., Seiler, N., Mey, J., Klee, D., Moller, M., Dalton, P.D., and Brook, G.A. Human neural cell interactions with orientated electrospun nanofibers *in vitro*. Nanomedicine **4,** 11, 2009.
45. Baiguera, S., Gaudio, C.D., Fioravanzo, L., Bianco, A., Grigioni, M., and Folin, M. *In vitro* astrocytes and cerebral endothelial cell response to electropun poly(ε-caprolactone) mats of different architecture. J Mate Sci Mater **21,** 1353, 2010.
46. East, E., de Oliveira, D.B., Golding, J.P., and Phillips, J.B. Alignment of astrocytes increases neuronal growth in three-dimensional collagen gels and is maintained following plastic compression to form a spinal cord repair conduit. Tissue Eng A **16,** 3173, 2010.
47. Discher, D.E., Janmey, P., and Wang, Y.-L. Tissue cells feel and respond to the stiffness of their substrate. Science **310,** 1139, 2005.
48. Georges, P.C., Miller, W.J., Meaney, D.F., Sawyer, E.S., and Janmey, P.A. Matrices with compliance comparable to that of brain tissue select neuronal over glial growth in mixed cortical cultures. Biophys J **90,** 3012, 2006.
49. Stokols, S., and Tuszynski, M.H. Freeze-dried agarose scaffolds with uniaxial channels stimulate and guide linear axonal growth following spinal cord injury. Biomaterials **27,** 443, 2006.
50. Cao, H., McHugh, K., Chew, S.Y., and Anderson, J.M. The topographical effect of electrospun nanofibrous scaffolds on the *in vivo* and *in vitro* foreign body reaction. J Biomed Mater Res A **93,** 1151, 2010.
51. Moses, O., Vitrial, D., Aboodi, G., Sculean, A., Tal, H., Kozlovsky, A., Artzi, Z., Weinreb, M., and Nemcovsky, C.E. Biodegradation of three different collagen membranes in the rat calvarium: a comparative study. J Periodontol **79,** 905, 2008.
52. Bölgen, N., Menceloğlu, Y.Z., Acatay, K., Vargel, I., and Pikin, E. *In vitro* and *in vivo* degradation of non-woven materials made of poly(ε-caprolactone) nanofibers prepared by electrospinning under different conditions. J Biomate Sci Polymer Ed **16,** 1537, 2005.
53. Hsu, J.-Y.C., and Xu, X.-M. Early profiles of axonal growth and astroglial response after spinal cord hemisection and implantation of Schwann cell-seeded guidance channels in adult rats. J Neurosci Res **82,** 472, 2005.
54. Wang, H.B., Mullins, M.E., Cregg, J.M., McCarthy, C.W., and Gilbert, R.J. Varying the diameter of aligned electrospun fibers alters neurite outgrowth and Schwann cell migration. Acta Biomater **6,** 2970, 2010.

Address correspondence to:
Sing Yian Chew, Ph.D.
School of Chemical and Biomedical Engineering
Nanyang Technological University
62 Nanyang Drive
Singapore 637459
Singapore

E-mail: sychew@ntu.edu.sg

Received: July 31, 2011
Accepted: January 3, 2012
Online Publication Date: February 7, 2012

This article has been cited by:

1. John D. Houle, Marie-Pascale Côté. 2013. Axon regeneration and exercise-dependent plasticity after spinal cord injury. *Annals of the New York Academy of Sciences* **1279**:1, 154-163. [CrossRef]
2. Fabio Zomer Volpato, Tobias Führmann, Claudio Migliaresi, Dietmar W. Hutmacher, Paul D. Dalton. 2013. Using extracellular matrix for regenerative medicine in the spinal cord. *Biomaterials* . [CrossRef]
3. Jo'an Bardy, Allen K. Chen, Yu Ming Lim, Selena Wu, Shunhui Wei, Han Weiping, Ken Chan, Shaul Reuveny, Steve K.W. Oh. 2013. Microcarrier Suspension Cultures for High-Density Expansion and Differentiation of Human Pluripotent Stem Cells to Neural Progenitor Cells. *Tissue Engineering Part C: Methods* **19**:2, 166-180. [Abstract] [Full Text HTML] [Full Text PDF] [Full Text PDF with Links]
4. Ana Paula Pêgo, Sarka Kubinova, Dasa Cizkova, Ivo Vanicky, Fernando Milhazes Mar, Mónica Mendes Sousa, Eva Sykova. 2012. Regenerative medicine for the treatment of spinal cord injury: more than just promises?. *Journal of Cellular and Molecular Medicine* **16**:11, 2564-2582. [CrossRef]
5. Raymund E. Horch, Ulrich Kneser, Elias Polykandriotis, Volker J. Schmidt, Jiaming Sun, Andreas Arkudas. 2012. Tissue Engineering and Regenerative Medicine - Where do we stand?. *Journal of Cellular and Molecular Medicine* n/a-n/a. [CrossRef]